RSC Advances

PAPER

View Article Online
View Journal | View Issue

Cite this: *RSC Adv.*, 2025, **15**, 43844

Anomalous Hall and multipiezo phenomena in a two-dimensional altermagnetic Janus Cr_2S_2Se

Abid Zaman, *[a] Salhah Hamed Alrefaee,[b] Hifsa Shahid,[c] Abduvali Sottarov,[d] S. G. Asadullayeva,[efg] Reem Alreshidi,*[h] Vineet Tirth[ij] and Ali Algahtani[ik]

The emergence of altermagnetism, which combines a compensated magnetic configuration with momentum-dependent spin band splitting, has introduced new opportunities for spintronic research. In particular, the integration of altermagnetism with multifunctional properties such as piezoelectricity, piezovalley coupling, and piezomagnetism that offers a promising route toward strain-engineered magneto-electronic devices. Motivated by this perspective, we explored the two-dimensional Janus monolayer Cr_2S_2Se using density functional theory. Our results reveal that the system is both thermodynamically and dynamically stable, while its magnetic ground state is antiferromagnetic with a Néel temperature of approximately 320 K. The electronic structure demonstrates an indirect band gap of about 0.14 eV and pronounced non-relativistic spin splitting (~0.46 eV) at the high-symmetry points, a clear hallmark of altermagnetic behavior. The lack of mirror symmetry in the Janus configuration further induces an out-of-plane piezoelectric response, yielding sizable piezoelectric coefficients ($e_{31} \approx 69.80$ pC m^{-1} and $d_{31} \approx 0.36$ pm V^{-1}). Additionally, we observed a strain-driven piezovalley effect, producing a valley polarization as large as 142 meV. Interestingly, carrier doping under applied strain activates a finite piezomagnetic response. The coexistence of these distinct functionalities such as altermagnetism, piezovalley, piezoelectricity, and piezomagnetism that's positions Cr_2S_2Se as a compelling candidate for strain-tunable valleytronic and spintronic applications. Importantly, its potential fabrication *via* methods such as mechanical exfoliation or chemical vapor deposition enhances the experimental feasibility of this material.

Received 25th September 2025
Accepted 29th October 2025

DOI: 10.1039/d5ra07306e

rsc.li/rsc-advances

1 Introduction

The discovery of altermagnetism has recently sparked considerable research interest because of its unconventional magnetic configuration. In this state, spin-polarized electronic bands appear without the need for relativistic interactions such as spin–orbit coupling (SOC).[1–4] Altermagnetism originates from a newly recognized magnetic phase that resembles collinear antiferromagnetism in real space but produces spin band splitting in momentum space, a characteristic typically associated with ferromagnets. Unlike traditional antiferromagnets, altermagnets preserve overall spin compensation while simultaneously allowing spin-selective electronic transport, owing to their symmetry-driven, non-relativistic spin-split bands. Since this splitting is generated by crystal symmetry combined with exchange interactions rather than SOC, its magnitude can surpass the energy scale commonly associated with relativistic effects.[1–3] An important implication of this mechanism is the ability to manipulate spin degrees of freedom without introducing macroscopic magnetization, thereby avoiding undesirable effects such as stray magnetic fields. As a result, altermagnetic systems are being recognized as promising candidates for a variety of frontier applications, including spintronic devices, chiral magnetic functionalities, and platforms for topological superconductivity.[4–6] Materials that were once categorized as conventional antiferromagnets, such as MnF_2 in the rutile phase[2] and RuO_2,[6] have been reclassified as altermagnets, and ongoing high-throughput computational

[a]*Department of Physics, Riphah International University, Islamabad 44000, Pakistan. E-mail: zaman.abid87@gmail.com*
[b]*Department of Chemistry College of Science Taibah University, Yanbu Governorate, Saudi Arabia*
[c]*Department of Electrical Engineering, College of Engineering, Qassim University, Unayzah, Saudi Arabia*
[d]*Department of Information Technology and Exact Sciences, Termez University of Economics and Service, Termez, Uzbekistan*
[e]*Institute of Physics, Ministry of Science and Education, Baku, AZ1143, Azerbaijan*
[f]*Azerbaijan State Oil and Industry University, 20 Azadlig Street, Baku, 1010, Azerbaijan*
[g]*Khazar University, Department of Physics and Electronics, Mahsati Str. 41, Baku, Az 1096, Azerbaijan*
[h]*Department of Physics, College of Science, Northern Border University, Arar, Saudi Arabia. E-mail: Reem.Alreshidi@nbu.edu.sa*
[i]*Mechanical Engineering Department, College of Engineering, King Khalid University, Abha 61421, Aseer, Kingdom of Saudi Arabia*
[j]*Centre for Engineering and Technology Innovations, King Khalid University, Abha 61421, Aseer, Kingdom of Saudi Arabia*
[k]*Research Center for Advanced Materials Science (RCAMS), King Khalid University, Guraiger, P.O. Box 9004, Abha-61413, Aseer, Kingdom of Saudi Arabia*

efforts continue to reveal new compounds with similar characteristics.[7,8]

Parallel to this development, the observation of long-range magnetism in the monolayer material CrI_3 initiated an upsurge of activity in the field of two-dimensional (2D) magnetism.[9] Since then, diverse families of 2D magnets have been reported, ranging from itinerant ferromagnets such as Fe_3GeTe_2 (ref. 10) to layered antiferromagnets like $FePS_3$,[11,12] and even noncollinear systems such as NiI_2.[13] More recent theoretical studies have proposed that certain 2D compounds can also host altermagnetic phases. Examples include V_2Se_2O and V_2Te_2O,[14,15] chromium oxychalcogenides such as Cr_2Te_2O and Cr_2Se_2O,[4] $(CrO)_2$,[16,17] and Cr_2SO.[18] Despite this growing body of work, the experimental confirmation and deeper theoretical understanding of altermagnetism in 2D systems remain limited. In addition, the ability to tune interlayer interactions in layered structures opens the possibility of driving topological phase transitions.[19,20] This raises a key question that has not been adequately explored: how does the layer degree of freedom give rise to novel physical responses in altermagnetic systems?

Mechanical strain has emerged as another effective approach for tailoring the properties of 2D materials.[21–24] When a lattice is subjected to external deformation, it can host a variety of emergent effects, including strain-driven topological phase transitions,[21–23,25,26] piezoelectricity,[27] and valley-related functionalities such as the piezovalley effect.[28,29] Among these, controlling topological phases *via* strain has been one of the most widely studied approaches. Piezoelectricity itself is an electromechanical phenomenon in which mechanical deformation leads to the generation of an internal electric potential, a property that is absent in centrosymmetric crystals.[27] In contrast to conventional ferrovalley materials, where time-reversal symmetry governs valley polarization, the altermagnetic monolayer V_2Se_2O demonstrates a different mechanism. Owing to its crystalline symmetry, it supports a process known as C-paired spin–valley locking (SVL), which protects valley states against scattering.[28] When a uniaxial strain is applied, this degeneracy is lifted, producing a strain-driven valley polarization referred to as the piezovalley effect. Moreover, chemical substitution in V_2Se_2O has been shown to introduce piezomagnetism, broadening its multifunctional nature.[29] This leads to an intriguing possibility: could this material also sustain piezoelectricity alongside other strain-driven functionalities, thus exhibiting what may be termed a "multipiezo effect"? Recent progress in Janus-type 2D structures suggests a pathway to realize such multifunctionality.[30,31] By breaking the out-of-plane mirror symmetry through compositional asymmetry, Janus monolayers naturally exhibit out-of-plane piezoelectric polarization. Extending this design principle to Cr_2S_2Se could enable the integration of piezoelectric, piezomagnetic, and piezovalley responses in a single system, offering a versatile multifunctional platform. In the present study, we provide a systematic analysis of the Cr_2S_2Se monolayer with a focus on its magnetic ordering, structural and mechanical stability, and the potential realization of multipiezo phenomena. Our results demonstrate how structural asymmetry, combined with strain engineering, can be exploited to tailor the functional responses of two-dimensional altermagnets. This work highlights promising opportunities for designing next-generation spintronic and valleytronic devices based on strain-modulated 2D altermagnetic materials.

2 Computational techniques

Here in we computed the different physical properties of altermagnet Cr_2S_2Se monolayer through VASP. The electron–ion interactions were modeled by means of the projector augmented-wave (PAW) method, and the exchange–correlation potential was described within the GGA as formulated by PBE. To capture the strong on-site Coulomb interactions associated with the localized 3d states of chromium atoms, we employed the DFT + U scheme with a Hubbard U value of 3.5 eV. The value of U is taken from the literature.[32,33] The plane-wave basis set was truncated at an energy cutoff of 500 eV. For sampling the Brillouin zone, a Monkhorst–Pack grid of 15 × 15 × 1 k-points was adopted during the optimization procedure. The relaxation process was carried out until the total energy difference between successive steps became smaller than 10^{-6} eV, and the residual atomic forces were minimized to less than 0.01 eV Å^{-1}. We considered the vacuum of 20 along out of plane direction to avoid interactions between periodic images. The magnetic ground state was identified by comparing the total energies of ferromagnetic and antiferromagnetic spin arrangements. The dynamic stability of the optimized structure was verified through phonon spectrum calculations, which were obtained using the PHONOPY package. Magnetocrystalline anisotropy energy (MAE) was evaluated by incorporating spin–orbit coupling (SOC) and computing the energy difference between magnetization aligned along the out-of-plane and in-plane directions. We estimate the temperature-dependent sub-lattice magnetization based on the Metropolis Monte Carlo simulations using the VAMPIRE software package.[34] To compute the magnetic transition temperature, we utilized the field-cooling Monte Carlo technique. In our calculations, we employed the field-cooling Monte Carlo method in which the system temperature is gradually reduced from the high-temperature paramagnetic state to near absolute zero. To minimize finite-size effects, we constructed a 100 × 100 × 1 supercell under periodic boundary conditions along both the x and y axes, resulting in a total of 10 000 magnetic atoms/sites in the simulated lattice. The thermal evolution of the sublattice magnetization was tracked at each temperature step. For accuracy and reproducibility, we adopted a temperature step of 1.2 K throughout the cooling process. At each temperature point, we performed Monte Carlo sampling for 1 000 000-time steps, ensuring adequate statistical convergence of the magnetization. The total magnetization was then obtained by averaging over all atomic sites in the lattice. In addition, uniaxial strain was systematically applied to investigate strain-driven functionalities such as piezovalley and piezomagnetic effects.

3 Results and discussion

The Cr_2S_2Se monolayer is composed of three atomic layers, where sulphur (S) atoms form the top surface, selenium atoms

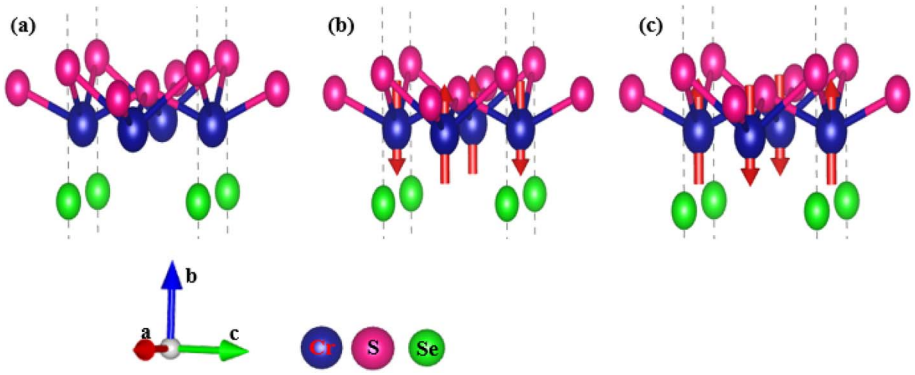

Fig. 1 (a) The unit cell of Cr_2S_2Se and (b) & (c) Possible AFM configuration.

occupy the bottom layer, and chromium atoms lie between them, giving rise to a Janus-type structure (Fig. 1a). This asymmetric stacking breaks the mirror symmetry along the out-of-plane direction, while the in-plane lattice maintains a tetragonal arrangement with fourfold rotational symmetry. The crystal belongs to the non-centrosymmetric space group *P4mm* (no. 99), which reflects reduced symmetry compared to centrosymmetric analogues. To identify the ground-state magnetic ordering, we compared the total energies of ferromagnetic (FM) and antiferromagnetic (AFM) configurations (Fig. 1b and c). In the AFM case, the two chromium atoms were arranged in a collinear fashion, with one spin oriented upward and the other downward. Energy calculations revealed that the AFM phase is more stable than the FM phase, with a difference of 270 meV per unit cell, indicating that the AFM configuration is the magnetic ground state. All further analyses were therefore performed using this AFM ordering.

The thermodynamic stability was evaluated through the formation energy, which was obtained as −2.21 eV per atom. The negative value of formation energy is the indication of thermodynamic stability.[35] To further confirm structural robustness, we computed the phonon dispersion spectrum

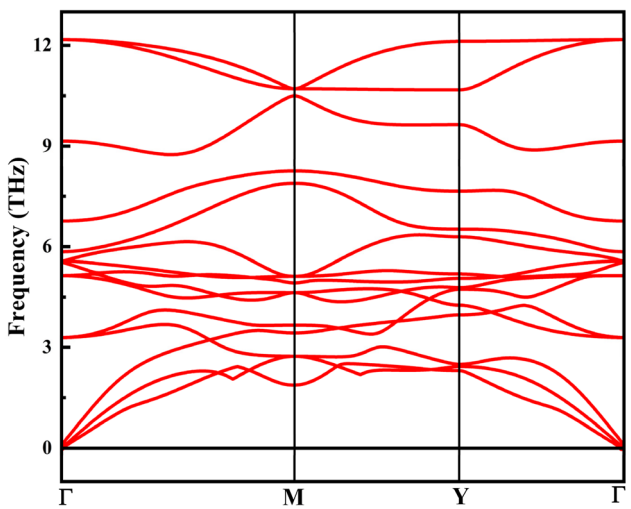

Fig. 2 Phonon dispersion curve for Cr_2S_2Se monolayer.

Fig. 2. The absence of imaginary frequencies across the Brillouin zone demonstrates dynamical stability.[36] Mechanical stability was examined through the calculation of elastic constants. The obtained values are $C_{11} = 119.9$ N m^{-1}, $C_{22} = 78.65$ N m^{-1}, and $C_{66} = 55.72$ N m^{-1}. According to the Born stability criteria, a 2D tetragonal system is mechanically stable when $C_{11} > 0$, $C_{66} > 0$ and $C_{11} > C_{12}$. These conditions are clearly satisfied, confirming that the Cr_2S_2Se monolayer is mechanically robust. Taken together, the thermodynamic, dynamical, and mechanical analyses demonstrate that the Cr_2S_2Se monolayer is a stable system, making it a realistic candidate for experimental synthesis and potential applications in 2D functional materials.

To further characterize the magnetic properties, we estimated the Néel temperature (T_n) of the V_2SeO Janus monolayer using the classical Heisenberg spin Hamiltonian:[26]

$$H_{ex} = -\sum_{i \neq j} J_{ij}(S_i \cdot S_j) - k_u(S_i \cdot e)^2 \quad (1)$$

$$n_\alpha = \frac{1}{N_\alpha}\sum_{i}^{N_\alpha} S_i \quad (2)$$

To determine the magnetic transition temperature of the Cr_2S_2Se monolayer, we employed a Monte Carlo simulation based on the field-cooling protocol. In this method, the system is first initialized in a high-temperature paramagnetic configuration, where thermal fluctuations dominate and spins are disordered. The temperature is then gradually reduced toward absolute zero, while the spin orientations are allowed to relax at each step. During the cooling process, the magnetization of individual sublattices is monitored, and the overall magnetization is obtained by averaging over all lattice sites. This procedure makes it possible to identify the critical temperature at which the long-range antiferromagnetic ordering disappears. From our simulations, the Néel temperature (T_N) was estimated to be around 320 K, a remarkably high value compared to many other two-dimensional antiferromagnets. Such a high transition temperature highlights the strength of the exchange interactions in this compound, confirming that the magnetic state remains robust well above room temperature. This

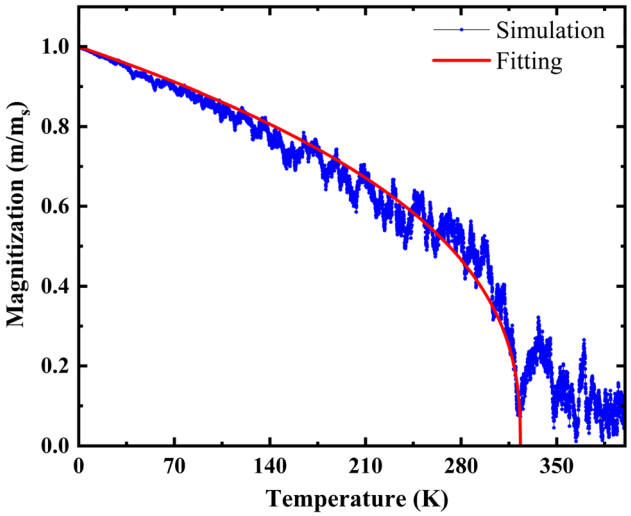

Fig. 3 Temperature dependent magnetization curve of the Janus for Cr_2S_2Se monolayer.

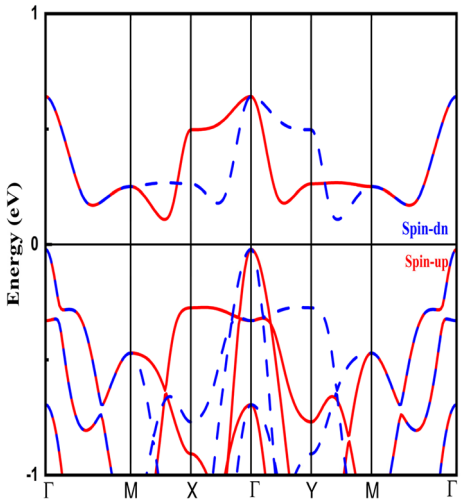

Fig. 4 The obtained band structure for Cr_2S_2Se monolayer.

property is particularly desirable for spintronic devices, which often require stable magnetic order under ambient operating conditions. The temperature-dependent evolution of the sublattice magnetization is presented in Fig. 3.

In addition to thermal stability, the magnetic anisotropy was evaluated through the calculation of the magnetocrystalline anisotropy energy (MAE), which determines the preferred spin orientation relative to the crystallographic axes. Our results reveal that the easy axis lies along the out-of-plane direction, with an energy barrier of 0.250 meV per Cr atom. A positive MAE value indicates that the spins favor alignment perpendicular to the plane of the monolayer. This out-of-plane preference is significant in two-dimensional magnets, where strong fluctuations can otherwise destabilize long-range ordering. The existence of an anisotropy barrier therefore provides an energetic constraint that helps maintain spin alignment, enhancing the material's potential for integration into spintronic applications such as magnetic memory and logic devices.

To gain deeper insight into the spin-resolved electronic behavior of the Cr_2S_2Se monolayer, we calculated its band structure. As shown in Fig. 4, the system behaves as a semiconductor, with an indirect band gap of approximately 0.14 eV located at the gamma point. A key feature of the dispersion is the clear imbalance between the spin channels: the spin-up and spin-down states no longer overlap, and this asymmetry is particularly evident at the high-symmetry X and Y points of the Brillouin zone. The magnitude of the splitting, quantified a $\Delta S = E^{\uparrow}(k) - E^{\downarrow}(k)$, reaches about 0.46 eV at the valence band maximum in these regions. What makes this observation remarkable is that such strong spin splitting arises even though the system has no net magnetization. This behavior is characteristic of altermagnetism, a recently recognized form of magnetic order. In conventional antiferromagnets, the opposite spins on different sublattices cancel out both in real space and in reciprocal space, leading to spin-degenerate electronic bands. By contrast, altermagnets preserve global time-reversal symmetry yet still exhibit momentum-resolved spin asymmetry. This is made possible by the combined action of lattice symmetry elements and spin rotations.

For Cr_2S_2Se, the tetragonal non-centrosymmetric crystal structure (space group *P4mm*) is central to this phenomenon. The absence of inversion symmetry, together with the specific antiferromagnetic spin arrangement, allows the electronic bands to acquire a momentum-locked spin polarization. Importantly, this spin splitting is non-relativistic in nature, meaning it occurs without requiring spin–orbit coupling (SOC). Instead, it is an intrinsic outcome of the symmetry-protected altermagnetic state. The result is that the two spin channels follow distinct pathways across the Brillouin zone, producing a highly anisotropic spin texture. This intrinsic spin asymmetry has profound technological consequences. It can enable momentum-selective spin transport and spin-filtering functionalities, effects usually associated with ferromagnetic systems or materials with strong SOC. However, in the case of Cr_2S_2Se, these properties emerge without introducing net magnetization. The absence of stray magnetic fields and the enhanced stability in nanoscale dimensions make this Janus monolayer an attractive platform for next-generation spintronic devices.

In its equilibrium configuration, the Janus Cr_2S_2Se monolayer does not possess any degenerate valleys. Herein, we applied uniaxial strain along the X-direction to examine whether the strain can induce a valley effect. Owing to the crystal symmetry, the X and Y axes are equivalent in the unstrained lattice; therefore, analyzing strain in the X-direction is sufficient. The resulting valley polarization, illustrated in Fig. 5, shows that the applied strain breaks the equivalence of the valleys and produces a noticeable energy difference, defined as $\Delta E_v = E_x - E_y$, between the X and Y points in the conduction valence bands. While in valence the piezovalley is not possible because maxima is present at gamma point instead of X and Y. Our calculations demonstrate that this valley splitting grows steadily with increasing strain, whether tensile or compressive.

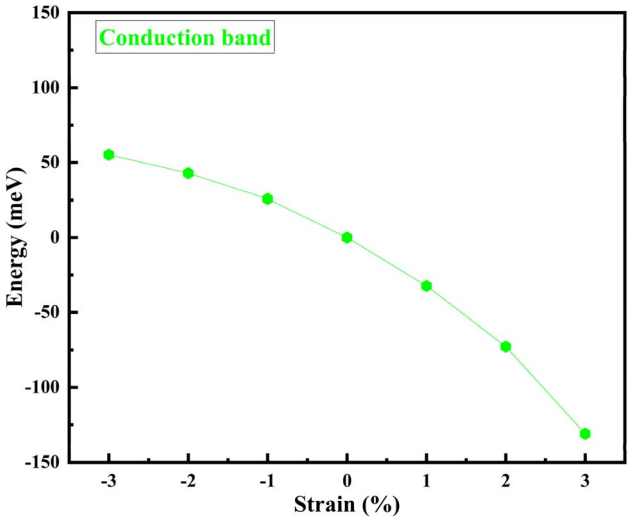

Fig. 5 The obtained Piezovalley graph for Cr_2S_2Se monolayer.

Under 3% tensile strain, the polarization reaches values of approximately 139 meV in the conduction band. Such strain-driven removal of valley degeneracy is recognized as the piezo-valley effect, a mechanical-response phenomenon analogous to piezoelectricity and piezomagnetism. The introduction of strain distorts the crystal arrangement, removing the diagonal reflection symmetry and enabling the electronic valleys located at *X* and *Y* points to develop separately. As the deformation becomes larger, this symmetry breaking becomes more pronounced, leading to an enhanced valley polarization. Remarkably, the maximum polarization obtained for Cr_2S_2Se (~131 meV) exceeds the values reported for a number of two-dimensional ferrovalley materials, including 2H-$FeCl_2$ (101 meV),[37] LaBrI (59 meV),[38] VSSe (85 meV),[39] and VSCl (57.8 meV).[14] It also outperforms the ~60 meV valley splitting observed in unstrained V_2Se_2O.[40] These findings confirm that valleys related by crystalline symmetry, often referred to as C-paired valleys, can be selectively tuned by mechanical deformation. Therefore, Janus Cr_2S_2Se emerges as a strong candidate for strain-controlled valleytronic applications, where valley polarization can be exploited as an additional degree of freedom for information processing in a magnetically compensated platform.

Applying uniaxial strain to the Janus Cr_2S_2Se monolayer not only lifts the valley degeneracy but also gives rise to a pronounced piezomagnetic response. The origin of this effect lies in the strain-driven valley polarization: the electronic states at the *X* and *Y* points of the Brillouin zone, which are equivalent in the unstrained case, shift to different energy levels once symmetry is broken. This energy separation creates an imbalance between valleys in both the conduction and valence bands. Upon introducing charge doping into a valley-asymmetric band profile, the Fermi energy can be adjusted in a way that it crosses exclusively with a single valley. Importantly, since each valley is associated with a specific spin character, filling only one valley results in a net spin imbalance. In this way, a finite magnetization (M) is generated, even though the pristine Cr_2S_2Se monolayer is globally antiferromagnetic, exhibiting no net moment under equilibrium conditions.

The induced magnetization through this mechanism can be formally described as:

$$M = \int_{E_F}^{\infty} \mu B \int \left[D^{\uparrow}(E,\varepsilon) - D^{\downarrow}(E,\varepsilon)\right] f(E,E_F)\mathrm{d}E \qquad (3)$$

Fig. 6 presents the evolution of the net magnetization in the Cr_2S_2Se monolayer as a function of uniaxial strain and hole doping concentration. The data reveal a clear trend: both increasing strain and higher doping levels lead to enhanced magnetization. A particularly intriguing feature is the opposite orientation of the induced magnetic moment under tensile *versus* compressive strain, which demonstrates that the direction of magnetic polarization can be reversibly tuned through mechanical deformation. In the regime of small strain, the induced magnetization varies almost linearly with strain, consistent with a direct piezomagnetic coupling. At larger strain values, however, the growth of magnetization slows down and eventually approaches saturation. The calculated magnitude of doping and strain-driven magnetic moments is comparable to that of other Janus antiferromagnetic monolayers, such as V_2Se_2O and V_2SeTeO,[36,37] highlighting the universality of this mechanism in related compounds. The distinct altermagnetic order in Cr_2S_2Se, characterized by momentum-resolved spin splitting without net magnetization in equilibrium, plays a central role in enabling this tunable piezomagnetic effect. In addition, the relatively weak magnetocrystalline anisotropy of the monolayer favors easy reorientation of spins under external perturbations, further enhancing controllability. Taken together, these properties establish Janus Cr_2S_2Se as a compelling platform for next-generation spintronic devices, where magnetic states can be dynamically tuned by strain engineering or electrostatic gating.

Piezoelectricity refers to the generation of spontaneous electric polarization when a crystal is subjected to mechanical

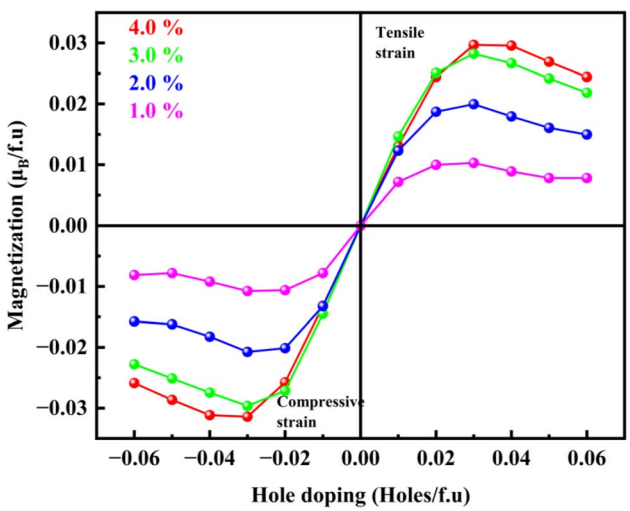

Fig. 6 The obtained piezomagnetism graph for Cr_2S_2Se monolayer.

deformation, and it can only occur in systems that lack inversion symmetry.[41–43] In the case of the Cr_2S_2Se monolayer, this condition is naturally satisfied due to its Janus-type atomic configuration, where sulfur and selenium layers occupy opposite sides of the central chromium layer. This intrinsic asymmetry breaks the out-of-plane mirror symmetry of the lattice, enabling a finite vertical piezoelectric effect. As a result, any in-plane strain can be effectively converted into an out-of-plane polarization response.

The piezoelectric effect is mathematically described by two third-rank tensors: the piezoelectric stress tensor e_{ijk} and the piezoelectric strain tensor d_{ijk}, defined as:

$$e_{ijk} = \frac{\partial P_i}{\partial \varepsilon_{jk}} = e_{ijk}^{\text{elc}} + e_{ijk}^{\text{ion}},$$
$$d_{ijk} = \frac{\partial P_i}{\partial \sigma_{jk}} = d_{ijk}^{\text{elc}} + d_{ijk}^{\text{ion}}, \quad (4)$$

where P_i denotes the polarization vector, ε_{jk} and σ_{jk} represent the strain and stress tensors, and the superscripts "elc" and "ion" account for the purely electronic and ionic contributions, respectively.[40,41] These tensors are related through the elastic constants (C_{mnjk}) by the relation:

$$e_{ijk} = d_{imn} \cdot C_{mnjk}$$

For the tetragonal structure of Cr_2S_2Se, symmetry reduces the number of independent tensor components. Importantly, the e_{31} component is nonzero, signifying that an in-plane strain directly induces an out-of-plane polarization. By employing density functional perturbation theory (DFPT), we determined e_{31} = 69.80 pC m^{-1}. Using this value along with the elastic constants C_{11} and C_{12}, the corresponding piezoelectric strain coefficient is obtained as:

$$d_{31} = \frac{e_{31}}{C_{11} + C_{12}} \quad (5)$$

yielding approximately 0.36 pm V^{-1}.

This value is comparable to that of other two-dimensional piezoelectrics such as $CrSSiN_2$ (0.28 pm V^{-1}),[44] significantly larger than $MoSiN_3H$ (0.058 pm V^{-1}),[45] though still smaller than few-layer 3R–MoS_2 (1.64 pm V^{-1}).[46] Taken together, these findings demonstrate that the Cr_2S_2Se monolayer exhibits a strong out-of-plane piezoelectric response, making it a promising candidate for nanoelectromechanical and energy-harvesting applications.

We now turn our attention to the cross-plane transport response, specifically the anomalous Hall effect (AHE). The Hall conductivity (σ_{xy}) is evaluated through the Kubo linear-response approach combined with Berry-phase formalism, where the integration of Berry curvature is performed throughout the Brillouin zone (BZ):

$$\sigma_{xy} = -\frac{e^2}{h}\sum_n \int_{\text{BZ}}^{\text{BZ}} \frac{\mathrm{d}k}{(2\pi)^3} f_n(k)\Omega_{n,k}(k) \quad (6)$$

Here, e denotes the elementary charge, (k) is the Fermi Dirac occupation factor, and corresponds to the Berry curvature associated with the n^{th} electronic band. The curvature itself is expressed as:

$$\Omega_{n,z}(k) = -\sum_n f_n \Omega_n(k) \quad (7)$$

$$\Omega_n(k) = -2\text{Im}\sum_{m\neq n} \frac{\langle u_{nk}|v_x|u_{mk}\rangle\langle u_{mk}|v_y|u_{nk}\rangle}{(E_{mk} - E_{nk})^2} \quad (8)$$

where $v_{x,y}$ are velocity operators, $u_{nk}(u_{mk})$ are the cell periodic Bloch functions, and $E_{nk}(E_{mk})$ denote the eigenenergy. For practical evaluation, we employed the Wannier interpolation scheme available in the Wannier90 package. This method constructs maximally localized Wannier functions (MLWFs) from Bloch states obtained in density functional theory (DFT) simulations. By Fourier transforming the Wannier Hamiltonian, an effective tight-binding representation is achieved, enabling accurate determination of Berry curvature and subsequent transport coefficients. The computed Hall conductivity of the monolayer is presented in Fig. 7. At a chemical potential of 0.75 eV, the value reaches −4.04 S cm^{-1} for the Cr_2S_2Se monolayer. Our calculated anomalous Hall conductivity is in close agreement with earlier works on 2D magnetic crystals. For instance, Wang *et al.* reported an AHC of about −3.8 S cm^{-1} for monolayer $Cr_2Ge_2Te_6$,[47] while Zhang *et al.* obtained a value near −4.2 S cm^{-1} in a study of transition-metal dichalcogenide-based ferromagnets[48] Beside it is reported to be 2.21 for antiferromagnetic Cr thin films.[49] The AHC is the key player among all the transverse transport coefficients, therefore to analyze the origin of AHC we calculated the Berry curvature in Cr_2S_2Se monolayer. Fig. 8 shows the distribution of the Berry curvatures over the 2D Brillouin zone (BZ) for the system at zero chemical potential. The blue and red colors represent the positive and negative Berry contributions. The positive or negative Berry contributions lead to positive or negative AHC. Here we can see that Berry contribution originated through high symmetry points K_y is very small and the negative Berry contribution

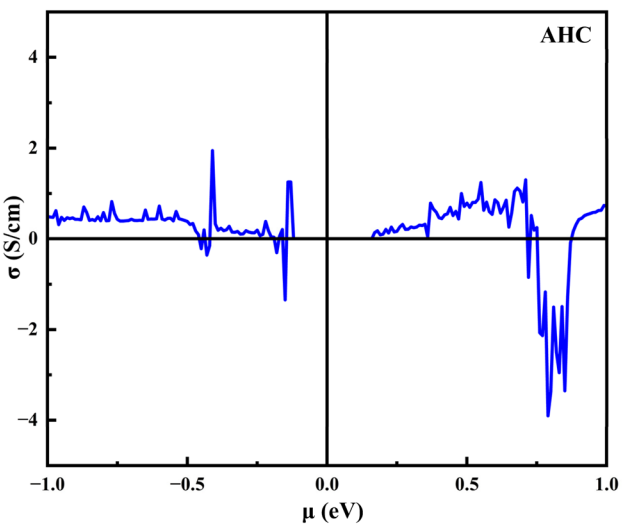

Fig. 7 The obtained anomalous Hall conductivity for Cr_2S_2Se monolayer.

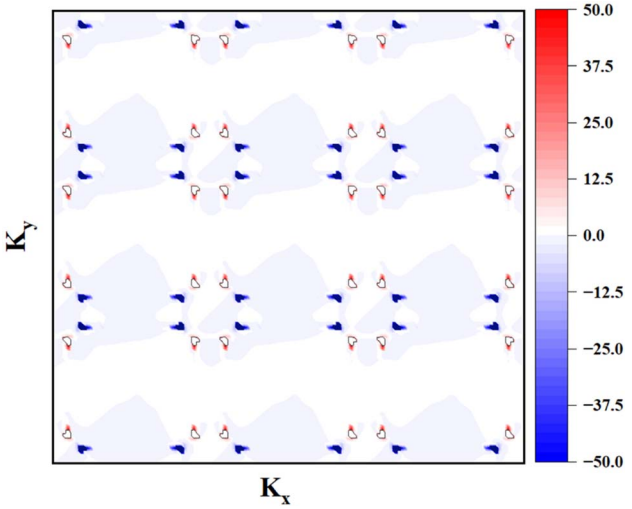

Fig. 8 The obtained Barry curvature graph for Cr_2S_2Se monolayer.

originated through K_x high symmetry points of the BZ is very high in system. This means that AHC at 0.75 eV having value of about -4.04 S cm^{-1} is mainly originated along K_x direction.

4 Conclusion

In this work, we performed an in-depth density functional theory (DFT) study of the Janus monolayer Cr_2S_2Se, focusing on its structural, magnetic, electronic, and multifunctional properties. Our calculations established that the ground state is antiferromagnetic, lying 270 eV lower in energy compared to the ferromagnetic arrangement. The material exhibits robust stability, as indicated by its negative formation energy (-2.21 eV per atom) and the absence of imaginary frequencies in the phonon spectrum. The predicted Néel temperature of about 320 K, derived using the Heisenberg spin Hamiltonian, suggests that the antiferromagnetic order remains intact well above ambient conditions, underscoring its feasibility for practical applications. Electronic band structure analysis revealed that Cr_2S_2Se is an indirect-gap semiconductor (0.14 eV), and importantly, it hosts a pronounced spin splitting of nearly 0.46 eV at the *X* and Y valleys in the valence band. This feature reflects its altermagnetic nature, where momentum-dependent spin polarization emerges from symmetry rather than relativistic spin–orbit effects. Such spin–valley coupling paves the way for a piezovalley effect: under applied uniaxial strain, the valley degeneracy is lifted, producing a valley polarization as large as 142 meV that is substantially larger than the thermal energy scale and higher than in several reported ferrovalley systems. The broken inversion symmetry of the Janus structure also imparts a finite out-of-plane piezoelectric response. Using density functional perturbation theory, we obtained a piezoelectric stress coefficient of $e_{31} = 69.80$ pC m^{-1} and a strain coefficient of $d_{31} = 0.36$ pm V^{-1}. These values demonstrate that Cr_2S_2Se is competitive with, or superior to, many other two-dimensional piezoelectric materials. Furthermore, by combining strain engineering with carrier doping, the valley-split states generate a finite net magnetization, giving rise to a tunable piezomagnetic effect. The induced magnetization strengthens with both doping level and strain magnitude and reverses orientation under compressive *versus* tensile strain, offering a reversible means of magnetic control.

Overall, Janus Cr_2S_2Se uniquely combines altermagnetism, piezoelectricity, piezovalley, and piezomagnetism in a single platform. This rare coexistence of multifunctional responses positions it as a promising candidate for future two-dimensional devices where strain, electric fields, or carrier doping can be used to dynamically control spin, valley, and polarization states. Considering that bulk analogues of Cr_2S_2Se and related compounds have already been synthesized, its experimental realization through chemical vapor deposition or exfoliation appears feasible, opening opportunities in next-generation strain-adaptive spintronic, valleytronic, and smart sensing technologies.

Conflicts of interest

The authors declare no conflict of interest.

Acknowledgements

The authors extend their appreciation to the Deanship of Research and Graduate Studies at King Khalid University for funding this work through the Large Research Project under the grant number RGP.2/198/46. The authors extend their appreciation to the Deanship of Scientific Research at Northern Border University, Arar, KSA for funding this research work through the project number "NBU-FFR-2025-3547-02".

References

1 S. Hayami, Y. Yanagi and H. Kusunose, Momentum-dependent spin splitting by collinear antiferromagnetic ordering, *J. Phys. Soc. Jpn.*, 2019, **88**(12), 123702.
2 L. D. Yuan, Z. Wang, J. W. Luo, E. I. Rashba and A. Zunger, Giant momentum-dependent spin splitting in centrosymmetric low-Z antiferromagnets, *Phys. Rev. B*, 2020, **102**(1), 014422.
3 L. Šmejkal, A. H. MacDonald, J. Sinova, S. Nakatsuji and T. Jungwirth, Anomalous hall antiferromagnets, *Nat. Rev. Mater.*, 2022, 7(6), 482–496.
4 Q. Cui, B. Zeng, P. Cui, T. Yu and H. Yang, Efficient spin Seebeck and spin Nernst effects of magnons in altermagnets, *Phys. Rev. B*, 2023, **108**(18), L180401.
5 L. Šmejkal, J. Sinova and T. Jungwirth, Emerging research landscape of altermagnetism, *Phys. Rev. X*, 2022, **12**(4), 040501.
6 L. Šmejkal, A. Marmodoro, K. H. Ahn, R. González-Hernández, I. Turek, S. Mankovsky, H. Ebert, S. W. D'Souza, O. Šipr, J. Sinova and T. Jungwirth, Chiral magnons in altermagnetic RuO 2, *Phys. Rev. Lett.*, 2023, **131**(25), 256703.

7 Z. F. Gao, S. Qu, B. Zeng, Y. Liu, J. R. Wen, H. Sun, P. J. Guo and Z. Y. Lu, AI-accelerated discovery of altermagnetic materials, *Natl. Sci. Rev.*, 2025, **12**(4), nwaf066.
8 X. Chen, Y. Liu, P. Liu, Y. Yu, J. Ren, J. Li, A. Zhang and Q. Liu, *arXiv preprint arXiv:*, 2023, **2307**, 12366.
9 B. Huang, G. Clark, E. Navarro-Moratalla, D. R. Klein, R. Cheng, K. L. Seyler, D. Zhong, E. Schmidgall, M. A. McGuire, D. H. Cobden and W. Yao, Layer-dependent ferromagnetism in a van der Waals crystal down to the monolayer limit, *Nature*, 2017, **546**(7657), 270–273.
10 Z. Fei, B. Huang, P. Malinowski, W. Wang, T. Song, J. Sanchez, W. Yao, D. Xiao, X. Zhu, A. F. May and W. Wu, Two-dimensional itinerant ferromagnetism in atomically thin Fe3GeTe2, *Nat. Mater.*, 2018, **17**(9), 778–782.
11 X. Wang, K. Du, Y. Y. Liu, P. Hu, J. Zhang, Q. Zhang, M. H. Owen, X. Lu, C. K. Gan, P. Sengupta and C. Kloc, Raman spectroscopy of atomically thin two-dimensional magnetic iron phosphorus trisulfide (FePS3) crystals, *2D Materials*, 2016, **3**(3), 031009.
12 J. U. Lee, S. Lee, J. H. Ryoo, S. Kang, T. Y. Kim, P. Kim, C. H. Park, J. G. Park and H. Cheong, Ising-type magnetic ordering in atomically thin FePS3, *Nano Lett.*, 2016, **16**(12), 7433–7438.
13 Q. Song, C. A. Occhialini, E. Ergeçen, B. Ilyas, D. Amoroso, P. Barone, J. Kapeghian, K. Watanabe, T. Taniguchi, A. S. Botana and S. Picozzi, Evidence for a single-layer van der Waals multiferroic, *Nature*, 2022, **602**(7898), 601–605.
14 H. Y. Ma, M. Hu, N. Li, J. Liu, W. Yao, J. F. Jia and J. Liu, Multifunctional antiferromagnetic materials with giant piezomagnetism and noncollinear spin current, *Nat. Commun.*, 2021, **12**(1), 2846.
15 Q. Cui, Y. Zhu, X. Yao, P. Cui and H. Yang, Giant spin-Hall and tunneling magnetoresistance effects based on a two-dimensional nonrelativistic antiferromagnetic metal, *Phys. Rev. B*, 2023, **108**(2), 024410.
16 X. Chen, D. Wang, L. Li and B. Sanyal, Giant spin-splitting and tunable spin-momentum locked transport in room temperature collinear antiferromagnetic semimetallic CrO monolayer, *Appl. Phys. Lett.*, 2023, **123**(2), 022402.
17 P. J. Guo, Z. X. Liu and Z. Y. Lu, Quantum anomalous hall effect in collinear antiferromagnetism, *npj Comput. Mater.*, 2023, **9**(1), 70.
18 S. D. Guo, X. S. Guo, K. Cheng, K. Wang and Y. S. Ang, Piezoelectric altermagnetism and spin-valley polarization in Janus monolayer Cr2SO, *Appl. Phys. Lett.*, 2023, **123**, 082401.
19 Y. Kim, P. Herlinger, P. Moon, M. Koshino, T. Taniguchi, K. Watanabe and J. H. Smet, Charge inversion and topological phase transition at a twist angle induced van Hove singularity of bilayer graphene, *Nano Lett.*, 2016, **16**(8), 5053–5059.
20 P. Li and T. Y. Cai, Two-dimensional transition-metal oxides Mn2O3 realized the quantum anomalous hall effect, *J. Phys. Chem. C*, 2020, **124**(23), 12705–12712.
21 P. Li and T. Y. Cai, Fully spin-polarized quadratic non-Dirac bands realized quantum anomalous Hall effect, *Phys. Chem. Chem. Phys.*, 2020, **22**(2), 549–555.
22 K. Wang, Y. Li, H. Mei, P. Li and Z. X. Guo, Quantum anomalous Hall and valley quantum anomalous Hall effects in two-dimensional d 0 orbital XY monolayers, *Phys. Rev. Mater.*, 2022, **6**(4), 044202.
23 P. Li, C. Wu, C. Peng, M. Yang and W. Xun, Multifield tunable valley splitting in two-dimensional MXene Cr 2 COOH, *Phys. Rev. B*, 2023, **108**(19), 195424.
24 J. Mutch, W. C. Chen, P. Went, T. Qian, I. Z. Wilson, A. Andreev, C. C. Chen and J. H. Chu, Evidence for a strain-tuned topological phase transition in ZrTe5, *Sci. Adv.*, 2019, **5**(8), eaav9771.
25 M. N. Blonsky, H. L. Zhuang, A. K. Singh and R. G. Hennig, Ab initio prediction of piezoelectricity in two-dimensional materials, *ACS Nano*, 2015, **9**(10), 9885–9891.
26 L. Bai, W. Feng, S. Liu, L. Šmejkal, Y. Mokrousov and Y. Yao, Altermagnetism: Exploring new frontiers in magnetism and spintronics, *Adv. Funct. Mater.*, 2024, **34**(49), 2409327.
27 J. Y. Li, A. D. Fan, Y. K. Wang, Y. Zhang and S. Li, Strain-induced valley polarization, topological states, and piezomagnetism in two-dimensional altermagnetic V 2 Te 2 O, V 2 STeO, V 2 SSeO, and V 2 S 2 O, *Appl. Phys. Lett.*, 2024, **125**(22), 222404.
28 S. D. Guo, X. S. Guo and G. Wang, Valley polarization in two-dimensional tetragonal altermagnetism, *Phys. Rev. B*, 2024, **110**(18), 184408.
29 P. Jiang, L. Kang, Y. L. Li, X. Zheng, Z. Zeng and S. Sanvito, Prediction of the two-dimensional Janus ferrovalley material LaBrI, *Phys. Rev. B*, 2021, **104**(3), 035430.
30 P. Zhao, Y. Dai, H. Wang, B. Huang and Y. Ma, Intrinsic valley polarization and anomalous valley hall effect in single-layer 2H-FeCl2, *ChemPhysMater*, 2022, **1**(1), 56–61.
31 H. Yang, M. Song, Y. Li, Y. Guo and K. Han, Ferromagnetism and valley polarization in Janus single-layer VSCl, *Phys. E Low-dimens. Syst. Nanostruct.*, 2022, **143**, 115341.
32 P. J. Guo, Z. X. Liu and Z. Y. Lu, Quantum anomalous hall effect in collinear antiferromagnetism, *npj Comput. Mater.*, 2023, **9**(1), 70.
33 S. D. Guo, X. S. Guo, K. Cheng, K. Wang and Y. S. Ang, Piezoelectric altermagnetism and spin-valley polarization in Janus monolayer Cr2SO, *Appl. Phys. Lett.*, 2023, **123**, 082401.
34 R. F. Evans, W. J. Fan, P. Chureemart, T. A. Ostler, M. O. Ellis and R. W. Chantrell, Atomistic spin model simulations of magnetic nanomaterials, *J. Phys.: Condens. Matter*, 2014, **26**(10), 103202.
35 C. Zhang, Y. Nie, S. Sanvito and A. Du, First-principles prediction of a room-temperature ferromagnetic Janus VSSe monolayer with piezoelectricity, ferroelasticity, and large valley polarization, *Nano Lett.*, 2019, **19**(2), 1366–1370.
36 H. Y. Ma, M. Hu, N. Li, J. Liu, W. Yao, J. F. Jia and J. Liu, Multifunctional antiferromagnetic materials with giant piezomagnetism and noncollinear spin current, *Nat. Commun.*, 2021, **12**(1), 2846.
37 Y. Zhu, T. Chen, Y. Li, L. Qiao, X. Ma, C. Liu, T. Hu, H. Gao and W. Ren, Multipiezo effect in altermagnetic V2SeTeO monolayer, *Nano Lett.*, 2023, **24**(1), 472–478.

38 Y. Q. Li, X. Zhang, X. Shang, Q. W. He, D. S. Tang, X. C. Wang and C. G. Duan, Magnetic and ferroelectric manipulation of valley physics in Janus piezoelectric materials, *Nano Lett.*, 2023, **23**(21), 10013–10020.

39 S. D. Guo, M. X. Wang, Y. L. Tao and B. G. Liu, Piezoelectric ferromagnetism in Janus monolayer YBrI: a first-principles prediction, *Phys. Chem. Chem. Phys.*, 2023, **25**(1), 796–805.

40 S. D. Guo, X. S. Guo, K. Cheng, K. Wang and Y. S. Ang, Piezoelectric altermagnetism and spin-valley polarization in Janus monolayer Cr2SO, *Appl. Phys. Lett.*, 2023, **123**, 082401.

41 S. D. Guo, X. S. Guo, X. X. Cai and B. G. Liu, Valley polarization transition driven by biaxial strain in Janus GdClF monolayer, *Phys. Chem. Chem. Phys.*, 2022, **24**(2), 715–723.

42 J. Liao, X. Ma, G. Yuan, P. Xu and Z. Yuan, Coexistence of in- and out-of-plane piezoelectricity in Janus XSSiN2 (X= Cr, Mo, W) monolayers, *Appl. Surf. Sci.*, 2023, **610**, 155586.

43 X. Cai, G. Chen, R. Li, Z. Pan and Y. Jia, Novel valleytronic and piezoelectric properties coexisting in Janus MoAZ 3 H (A= Si, or Ge; Z= N, P, or As) monolayers, *J. Phys. Chem. C*, 2024, **12**(13), 4682–4689.

44 H. Hallil, W. Cai, K. Zhang, P. Yu, S. Liu, R. Xu, C. Zhu, Q. Xiong, Z. Liu and Q. Zhang, Strong piezoelectricity in 3R-MoS2 flakes, *Adv. Electron. Mater.*, 2022, **8**(7), 2101131.

45 H. Lin, J. Si, X. Zhu, K. Cai, H. Li, L. Kong, X. Yu and H. H. Wen, Structure and physical properties of CsV 2 Se 2− x O and V 2 Se 2 O, *Phys. Rev. B*, 2018, **98**(7), 075132.

46 J. You, J. Pan, S. L. Shang, X. Xu, Z. Liu, J. Li, H. Liu, T. Kang, M. Xu, S. Li and D. Kong, Salt-assisted selective growth of H-phase monolayer VSe2 with apparent hole transport behavior, *Nano Lett.*, 2022, **22**(24), 10167–10175.

47 C. Wang, X. Liu, L. Kang, B. L. Gu, Y. Xu and W. Duan, First-principles calculation of nonlinear optical responses by Wannier interpolation, *Phys. Rev. B*, 2017, **96**(11), 115147.

48 J. H. Han, M. Kwak, Y. Kim and J. Cheon, Recent advances in the solution-based preparation of two-dimensional layered transition metal chalcogenide nanostructures, *Chem. Rev.*, 2018, **118**(13), 6151–6188.

49 H. Chen, Z. Feng, H. Yan, P. Qin, X. Zhou, H. Guo, X. Wang, H. Wu, X. Zhang, Z. Meng and Z. Liu, Anomalous Hall effect in antiferromagnetic Cr thin films, *Phys. Rev. B*, 2021, **104**(6), 064428.